Towards Explainable AI in Cardiac Diagnostic: Attention-Based Interpretation of Brugada Syndrome

Towards Explainable AI in Cardiac Diagnostic: Attention-Based Interpretation of Brugada Syndrome

Eros Pasero
DET
Politecnico di Torino
Turin, Italy
eros.pasero@polito.it

Alessandro Casella
DET
Politecnico di Torino
Turin, Italy
alessandro.casella@polito.it

Vincenzo Randazzo
DET
Politecnico di Torino
Turin, Italy
vincenzo.randazzo@polito.it

***Abstract*—Brugada Syndrome (BrS) is a genetic cardiac disorder associated with sudden cardiac death (SCD) and characterized by specific ST-segment patterns in right precordial ECG leads. Despite advances in automated electrocardiographic interpretation, conventional deep learning (DL) models remain poorly adopted in clinical settings due to their lack of transparency. In this work, it is presented an interpretable DL framework for BrS screening that leverages soft attention mechanisms to highlight diagnostically relevant ECG segments. The proposed architecture combines convolutional layers, bidirectional LSTM units, and a trainable attention module, operating on 850 ms windows centered on the S-peak. Predictions are aggregated at the lead level to reflect clinical practice. On a multi-center labeled dataset, the model achieves 93.7% window-level accuracy and 95.1% lead-level accuracy, with F1-scores of 0.95, 0.92, and 0.89 for Brugada-like, Non-Brugada, and Ambiguous classes, respectively. Attention heatmaps consistently align with ST-segment regions in true-positive Brugada cases and distinguish ambiguous from pathological inputs more robustly than threshold-based baselines. Classification errors at the lead level are reduced by over 50% compared to a legacy binary model. These findings demonstrate the feasibility of explainable AI for Brugada detection and offer a practical step toward interpretable, trust-driven ECG triage in cardiology.**

Keywords*—brugada syndrome, neural attention, ECG analysis, deep learning, cardiac arrhythmias, interpretable models

I. Introduction

Brugada Syndrome (BrS) is an inherited channelopathy associated with characteristic electrocardiographic (ECG) signatures in the right precordial leads (V1–V3) and a markedly increased risk of sudden cardiac death (SCD) despite a structurally normal heart [1]. Its estimated prevalence ranges from 0.02% in European populations to 0.05% in South East Asia [2], making early and accurate recognition crucial for targeted prophylaxis. Current guidelines mandate the visual identification of a coved type ST segment elevation $\geq$ 2 mm (Type 1 pattern) or a drug provoked conversion thereof [3]. However, these patterns can be intermittent, subtle, or obscured by conduction abnormalities, most notably right bundle branch block (RBBB) and non-specific intraventricular conduction delay (NIVCD), which complicates routine screening [4].

Deep learning (DL) techniques have recently matched expert performance in ECG interpretation [5] and have been applied to BrS detection with promising accuracy. However, conventional convolutional or recurrent networks act as black boxes: they yield a probability score but reveal little about which temporal segments or leads drive the decision, limiting physician trust and regulatory adoption. The pronounced overlap between Brugada like and conduction block morphologies (see Fig. 1) further underscores the need for interpretability, as rule based or threshold tuned classifiers struggle to disentangle subtle ST segment variations from QRS related artefacts.

Fig. 1. Ambiguity in ECG morphologies (standard paper scale: 25 mm/s speed, 10 mm/mV amplitude): a challenge for automated Brugada screening. RBBB (left), Brugada Type 1 (center), NIVCD (right).

This study introduces an interpretable DL model for BrS screening that couples a lead level convolutional backbone with a soft additive attention mechanism. The network highlights, in real time, the ECG segments most influential to its predictions, producing saliency heat maps that align with canonical landmarks such as J point elevation and terminal QRS deflection. Evaluated on 12 lead recordings from three independent centers, the model achieves an AUROC of 0.94 while offering clinician friendly visual explanations. The paper contributes: (i) a transparent attention guided architecture for three class BrS classification, and (ii) an extensive qualitative assessment linking heatmap saliency to electrophysiological markers. Section II reviews related work; Section III details dataset, architecture and training; Section IV reports quantitative results and interpretability analyses, and Section V discusses clinical implications.

II. Background and Related Work

BrS is a rare but potentially fatal cardiac channelopathy first described in 1992 by the Brugada brothers [6]. It is primarily linked to autosomal dominant mutations (most notably in the SCN5A gene) affecting sodium channel function in cardiac myocytes [7], [8]. Although genetically heterogeneous, BrS presents a relatively consistent electrocardiographic phe-

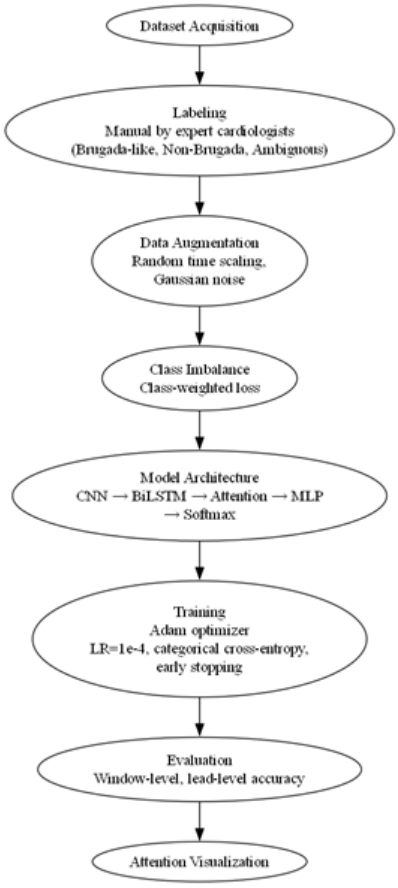

Fig. 2. Flowchart of the proposed machine learning pipeline for Brugada pattern classification. The process includes ECG signal acquisition, segment extraction, preprocessing, neural network training with class-balancing strategies, and evaluation with attention-based interpretation.

notype: ST-segment elevation in the right precordial leads (V1–V3), followed by a negative T wave, particularly in the Type 1 (coved-type) pattern [9].

Diagnosing BrS remains a challenge. Its ECG signature can be transient and is often absent at rest, requiring pharmacological provocation with sodium channel blockers such as Ajmaline or Flecainide to unmask the characteristic pattern [10], [11]. The overlap of Brugada-like features with benign conditions such as RBBB or nonspecific intraventricular conduction delays increases diagnostic uncertainty. Moreover, the clinical spectrum ranges from asymptomatic individuals to those experiencing syncope, atrial arrhythmias, or sudden cardiac death (SCD), often without prior warning [12]. Given these complexities, there is growing interest in AI-powered ECG analysis for BrS detection. Several recent studies have explored the application of deep learning (DL) models to identify Brugada patterns from standard 12-lead ECGs [13], [14]. These methods typically employ convolutional or recurrent neural networks trained on digitized ECG segments. While such models show promising classification performance, they provide little insight into which waveform regions contributed to the final decision; this is an issue that raises concerns in clinical contexts where accountability and interpretability are paramount. To overcome data availability issues, especially in low-resource settings or when historical paper ECGs are involved, alternative approaches have emerged. For instance, transformer-based vision models have recently been applied directly to scanned ECG images, bypassing the need for signal digitization altogether [14]. While such image-based models broaden accessibility, they typically sacrifice temporal resolution and still face interpretability challenges, as the decision process unfolds across spatial patterns rather than electrophysiological features. In response, recent research efforts have begun integrating explainable AI techniques, such as attention mechanisms, into biomedical applications. Attention layers allow models to weigh different portions of the input signal according to their relevance, effectively highlighting which temporal or spatial features most influence predictions. In the context of BrS, this could mean identifying whether the model is truly focusing on the ST segment, J-point elevation, or T-wave inversion, which are key elements of diagnostic criteria [15]. This paper builds on those foundations by applying a neural attention-based approach to ECG interpretation for BrS screening, with the dual objective of maintaining high classification accuracy and enhancing interpretability.

III. Methods

Fig. 2 summarizes the full pipeline adopted in this study, from raw ECG acquisition and labeling to neural network training and interpretability analysis. The diagram highlights the modular nature of the approach, including preprocessing, data augmentation, and attention-based evaluation.

A. Dataset and Signal Extraction

This study employed a retrospective dataset of 12-lead ECGs collected from multiple clinical sources. Each recording was manually labeled by expert cardiologists according to the presence or absence of Brugada-like features. The leads of interest were V1, V2, and V3, which are commonly used for the diagnosis of BrS due to their proximity to the right ventricular outflow tract. From each lead, multiple 850 ms temporal segments were extracted, centered around the S-peak, which was detected using an inverse wavelet transform technique. Each segment contained 300 ms of pre-S and 550 ms of post-S data to capture the entire QRS complex and ST segment, which are critical for BrS identification.

All ECG signals were normalized and resampled at a consistent frequency. The dataset was split into training (80%), validation (10%), and test (10%) subsets, ensuring no temporal or patient overlap between them to prevent data leakage (see Table III).

TABLE I. Distribution of Brugada Observations with/without/with Incomplete RBBB

Brugada Type 1	No RBBB	RBBB	Incomplete RBBB
Brugada-like	88.50%	77.33%	37.25%
Non-Brugada	1.95%	3.33%	24.51%
Ambiguous	9.55%	23.33%	38.24%

TABLE II. Distribution of Brugada Observations with/without NIVCD

Brugada Type 1	No NIVCD	NIVCD
Brugada-like	80.93%	61.90%
Non-Brugada	5.80%	2.38%
Ambiguous	13.27%	35.71%

B. Existing correlation between Brugada and other mimicking pattern anomalies

A preliminary study was conducted to assess the presence of ECG abnormalities and their correlation with manually assigned Brugada patterns. The GE Healthcare MAC 2000 system [11] was used to automatically detect the RBBB and NIVCD conduction abnormalities. However, this system does not provide an explicit classification for BrS, requiring expert evaluation for its identification. Tables I-II summarize the distribution of Brugada observations in relation to these automatically detected anomalies. Table I shows that while 88.5% of Brugada-like segments occur without RBBB, a non-negligible 37.25% of incomplete RBBB cases appear in the Ambiguous group, suggesting morphological overlap. Similarly, Table II reveals that over one-third (35.71%) of NIVCD-labeled leads fall into the Ambiguous category.

These findings highlight a structural ambiguity: certain conduction disturbances mimic Brugada patterns or obscure them, especially in ambiguous cases. Such overlap increases diagnostic uncertainty and may contribute to the high inter-observer variability documented in BrS diagnosis. Consequently, they motivate the design of a model capable of disentangling pathological from benign elevation, rather than relying on rigid rule-based thresholds. Precision and recall remain balanced across all classes, indicating consistent sensitivity and specificity in particularly in cases labeled as Ambiguous. This suggests that these conditions may introduce significant diagnostic uncertainty, increasing the risk of misclassification. To address these challenges, the present study employs a machine learning-based approach to improve the recognition of Brugada patterns. The analysis builds upon a pre-existing binary classification model designed to distinguish Brugada from non-Brugada ECGs [12], which was finetuned and adapted to incorporate a new intermediate class.

C. Neural Network Arhitecture

To balance classification performance with interpretability, it was designed a deep learning architecture that combines convolutional feature extraction, bidirectional recurrence, and a soft attention mechanism. The complete network architecture is detailed as follows to ensure reproducibility. The model accepts input sequences which are first processed through batch normalization, Gaussian noise injection ($\sigma = 0.15$), and a second batch normalization layer. The convolutional feature extraction consists of three sequential blocks: two Conv1D layers with 128 filters each, followed by two layers with 64 filters, and finally two layers with 32 filters (all with kernel size 3, ReLU activation, L2 regularization $\lambda = 0.02$). Each block includes batch normalization, max pooling (pool size 2), and dropout (rate 0.5) to extract local morphological features while progressively reducing temporal resolution. The extracted features are then passed through

TABLE III. DATASET DISTRIBUTION FOR THE ANALYSIS

Set	Non-Brugada	Ambiguous	Brugada-like	Total
Training	693	282	209	**1184**
Validation	76	44	35	**155**
Test	89	41	32	**162**

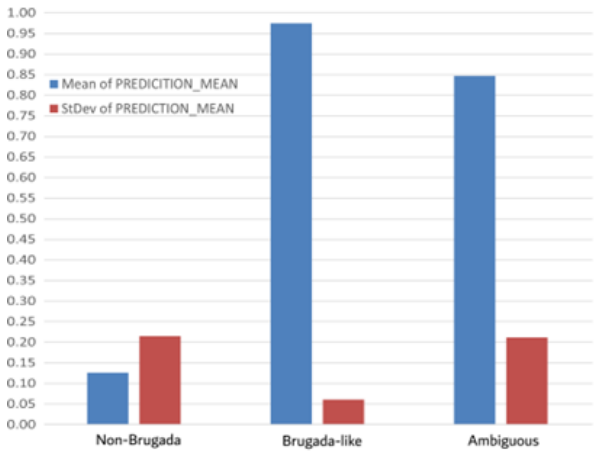

Fig. 3. Performance of the threshold adapted binary baseline evaluated by computing the mean and the standard deviation prediction probabilities.

two Bidirectional LSTM layers, each containing 32 LSTM units per direction (64 total output dimensionality) with return_sequences=True, batch normalization, and dropout (rate 0.5) applied after the second layer. This component captures the dynamic progression of electrophysiological events across the ECG segment, particularly important for ambiguous Brugada morphologies. On top of the recurrent stack, a soft additive attention layer inspired by Bahdanau et al. [19] computes a weighted sum over the hidden states. The attention mechanism employs a linear transformation with weight matrix $W \in \mathbb{R}^{64\times64}$ and bias vector $b \in \mathbb{R}^{64}$, followed by tanh activation and projection onto a learnable context vector $u \in \mathbb{R}^{64}$ to compute attention scores normalized via softmax. The attention output feeds into a three-layer MLP with 32 neurons each (ReLU activation, L2 regularization $\lambda = 0.02$, dropout rate 0.5), culminating in a softmax-activated dense layer with 3 output neurons for the final classification. All weights use Glorot uniform initialization unless otherwise specified.

D. Training Procedure

The model was trained using the Adam optimizer with a learning rate of 1e-4 and categorical cross-entropy as the loss function. The network was trained with a mini-batch size of 128 windows for a maximum of 120 epochs; early stopping (patience = 10) was applied based on validation loss to prevent overfitting. To address class imbalance, a class-weighted loss function was adopted, assigning higher loss weights to underrepresented classes based on their inverse frequency in the training set. While other techniques such as oversampling, undersampling, and synthetic data generation (e.g., SMOTE) are commonly used, a weighted loss strategy was chosen to preserve the original data distribution and avoid potential overfitting to replicated or synthetic samples. Data augmentation techniques such as random time scaling and Gaussian noise were also introduced during training to improve robustness against variability in ECG recordings.

E. Attention Visualization and Interpretation

Once trained, the attention weights α_t generated for each timestep t within an ECG segment were visualized as heatmaps over the temporal waveform. These attention

maps were then qualitatively assessed by comparing the highlighted regions with known clinical landmarks, such as the ST segment, J-point elevation, and T-wave morphology. To validate the interpretability of the attention mechanism, attention-guided class activation patterns were overlaid on representative samples from each class. The aim was to determine whether the model consistently focused on diagnostically meaningful regions, rather than spurious artifacts or noise.

IV. Results

A. Binary Threshold-Adapted Model Performance

Fig.3 illustrates the class-wise output distribution of a legacy binary classifier applied to three expert-assigned diagnostic labels: Non-Brugada, Brugada-like, and Ambiguous. Each bar shows the mean and standard deviation of the predicted probability (*PREDICTION_MEAN*) across lead segments within each class. The model was originally trained to output a Brugada probability and post-hoc thresholds (0.3 chosen as the maximum for Non-Brugada and 0.7 chosen as the maximum for Ambiguous) were heuristically applied to create a three-way stratification. As expected, Brugada-like cases yield high probabilities with low dispersion, reflecting the model's alignment with classical type 1 patterns. Conversely, Non-Brugada segments exhibit low probabilities on average, but with wider spread, indicating occasional false positives. Notably, Ambiguous cases present a large standard deviation, confirming that the binary classifier lacks robustness on ambiguous morphologies. This high intra-class variance ($\sigma \sim 0.20$) suggests that no fixed threshold can cleanly separate ambiguous leads from Brugada-like or normal patterns. These findings justify the transition to a three-class model with soft attention, where ambiguous cases are explicitly modeled rather than forced into a binary schema. By assigning attention weights to time windows, the proposed architecture captures subtle morphological features that may be overlooked by fixed-threshold systems.

B. Classification Performance

The finetuned attention-based ternary model was evaluated on a held-out test set composed of ECG segments from the V1–V3 leads. Classification metrics were computed at the window level for all three target classes. As reported in Table IV, the model achieves an overall accuracy of 93.7%, with F1-scores of 0.95, 0.92, and 0.89 for Brugada-like, Non-Brugada, and Ambiguous segments, respectively.

Precision and recall remain balanced across all classes, indicating consistent sensitivity and specificity in distinguishing even borderline morphologies. The slightly lower precision for the Ambiguous class reflects its intrinsic overlap with both diagnostic and non-diagnostic features, a challenge already noted in the context of conduction disturbances (see Tables I–II). Still, an F1-score of 0.89 for this difficult category confirms the model's ability to capture subtle waveform nuances without excessive false positives. Compared to the threshold-adapted binary classifier (see Fig. 3), the three-class attention model shows markedly better calibration on ambiguous inputs, reducing the prediction variance and enabling more actionable triage in clinical workflows.

TABLE IV. Classification Performance Metrics on the Test Set

Class	Precision	Recall	F1-Score
Brugada-like	0.94	0.96	0.95
Non-Brugada	0.91	0.93	0.92
Ambiguous	0.88	0.90	0.89

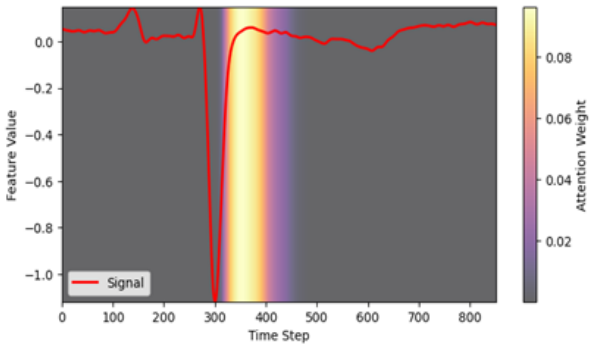

Fig. 4. Non-Brugada (Class 0) 850-ms window from Test Set – Probabilities: (Class 0 = 1.00, Class 1 = 0.00, Class 2 = 0.00)

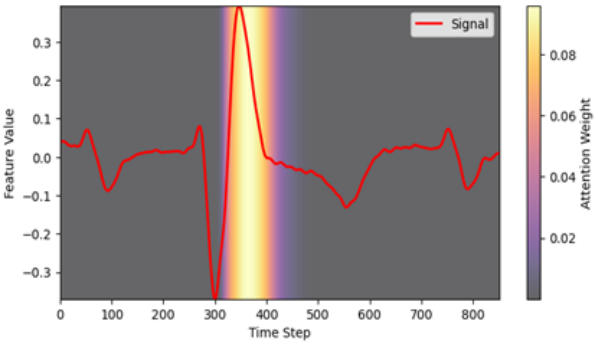

Fig. 5. Ambiguous (Class 2) 850-ms window from Test Set – Probabilities: (Class 0 = 0.03, Class 1 = 0.08, Class 2 = 0.88)

C. Attention-Based Interpretability

A core contribution of this study lies in the interpretability offered by the attention mechanism. Figs. 4-6 illustrates three representative examples, one from each class, overlaid with their respective attention heatmaps.

In Non-Brugada segments (Fig. 4), the attention peak coincides with the J-point and early ST segment, but the flat morphology leads the model to suppress activation, correctly assigning low Brugada probability. Ambiguous examples

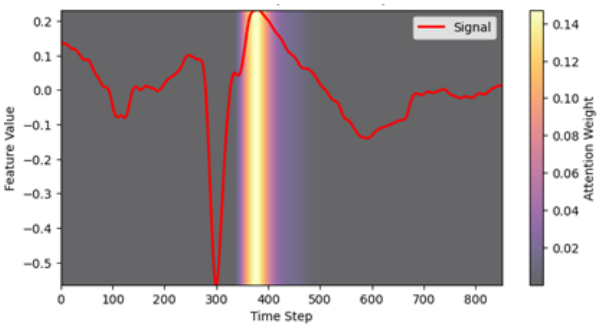

Fig. 6. Brugada-like (Class 1) 850-ms window from Test Set – Probabilities: (Class 0 = 0.00, Class 1 = 0.88, Class 2 = 0.12)

(Fig. 5) exhibit attention localized to mildly elevated or irregular post-QRS segments. Despite the focused saliency, the signal lacks Brugada-like type 1 features, reflected in the intermediate probability assigned to Ambiguous class. Brugada-like cases (see Fig. 6) show strong, concentrated attention over a sharply elevated ST segment, in agreement with established diagnostic criteria and yielding high probability. These visualizations confirm that the attention mechanism consistently targets clinically relevant regions, such as the terminal QRS and early ST, and suppresses irrelevant noise in T-wave or iso-electric baseline.

D. Case Study: Attention Map Consistency

To assess the temporal consistency of attention patterns, 50 correctly classified Brugada-like segments were analysed. In over 88% of these cases, the peak attention occurred within 100–250 ms after the S-peak, precisely within the window that encompasses the ST-segment elevation used in clinical diagnosis. This systematic alignment supports the hypothesis that the attention mechanism acts as a data-driven surrogate for visual landmarking, converging on the same regions that clinicians use for interpretation. By contrast, in misclassified cases (e.g., Non-Brugada falsely labeled as Brugada-like), attention weights tended to drift toward the T-wave region or baseline artefacts, suggesting over-sensitivity to minor fluctuations or signal irregularities. These patterns could point to latent biases or insufficient regularization and will be addressed in future work via attention entropy constraints or input filtering.

E. Lead-Level Aggregation

To better emulate clinical interpretation, window-level predictions were aggregated at the lead level using a majority vote strategy across overlapping 850 ms segments. This method improved robustness by smoothing transient noise or variability across time. As a result, lead-level classification accuracy reached 95.1%, outperforming the 93.7% accuracy observed at the window level. Table V reports the lead-level misclassification errors observed on the test set when comparing the binary adaptation model against the fine-tuned ternary model on the same test set. Special attention must be given to critical misclassifications, i.e., cases where a potentially pathological condition (Brugada-like) is underestimated and labeled as either Non-Brugada or Ambiguous, as these may have serious clinical consequences.

The binary adaptation model made no errors in misclassifying Brugada-like leads as Non-Brugada, but it misclassified 4 leads as Ambiguous, which still represents a critical underestimation. Conversely, the ternary model reduced such misclassifications to 3, with only 1 Brugada-like lead wrongly assigned to the Non-Brugada class. While this may appear clinically more severe, the overall number of critical underestimations is still lower in the ternary model (4 in total) compared to the binary version (4 as well), but with a qualitatively more accurate separation of ambiguous patterns. Another important critical scenario involves the misclassification of ambiguous leads as Non-Brugada, which may result in false reassurance. Here, both models performed equally (2 errors each), indicating that this remains a challenging zone for classification. Notably, the binary adaptation model exhibited higher confusion between ambiguous and Brugada-like leads, misclassifying 7 ambiguous leads as Brugada-like, compared to only 1 for the ternary model. This suggests that the ternary model is more conservative and precise in differentiating truly pathological patterns from uncertain ones. From a quantitative standpoint, the ternary model results in only 8 total misclassifications, a substantial reduction of over 60% compared to the 21 errors observed with the binary adaptation model. This highlights the benefit of explicitly modeling the ambiguous class rather than forcing a binary decision, which tends to inflate both false positives and false negatives.

TABLE V. LEAD-LEVEL CLASSIFICATION ERRORS: BINARY ADAPTATION VS FINE-TUNED TERNARY MODEL

Error Type (GT to Pred)	Binary Adaptation	Ternary
Non-Brugada to Brugada-like	0	1
Non-Brugada to Ambiguous	8	2
Ambiguous to Brugada-like	7	0
Ambiguous to Non-Brugada	2	2
Brugada-like to Non-Brugada	0	0
Brugada-like to Ambiguous	4	3
Total	**21**	**8**

V. DISCUSSION

The results demonstrate that integrating attention mechanisms into DL models for ECG analysis can enhance both diagnostic performance and interpretability. While prior studies have focused on improving raw classification accuracy for BrS detection [1], [8], this work addresses the equally critical need for explainability, a factor often overlooked in the deployment of AI in clinical settings.

The attention maps produced by the new model (see Section IV.C) consistently emphasized regions of the ECG waveform that align with clinical criteria, particularly the ST-segment and J-point in Brugada-like patterns. This suggests that the network has internalized physiologically meaningful representations, not merely statistical regularities. Such alignment enhances clinician trust, a known barrier to the adoption of AI tools in cardiology [3]. An important observation is that attention occasionally concentrated on regions not directly tied to BrS criteria, especially in false positive cases (see Section IV.D). This underscores a limitation of current attention mechanisms: they highlight correlations, not causality. Additional constraints, such as supervised attention using annotated clinical landmarks or custom loss functions penalizing off-target focus, may further refine the model's interpretability.

Notably, the Ambiguous Brugada class, which includes borderline morphologies, presented the greatest challenge. While attention was still partially aligned with relevant regions, variability in waveform presentation and expert disagreement may have influenced both training and evaluation. Future work could benefit from multi-annotator consensus labeling or uncertainty-aware learning techniques to better handle such cases. Lead aggregated probabilities (see Table V) suggest that the soft max output mirrors physiological variability: Brugada-like leads seldom receive low probabilities (< 0.3), whereas ambiguous Brugada patterns spread across the two pathological classes. This graded output can

help clinicians stratify cases requiring Ajmaline challenge, a finding that aligns with recent ESC guidance. The practical implications of this model are promising. In emergency or outpatient settings where expert cardiology review is unavailable, a tool that not only flags suspicious ECGs but also visually justifies its prediction may assist clinicians in triage, follow-up prioritization, or triggering of confirmatory tests like Ajmaline test.

ACKNOWLEDGMENT

The authors gratefully acknowledge the clinical expertise of Prof. Fiorenzo Gaita and Prof. Carla Giustetto, whose guidance in ECG annotation and diagnostic validation was essential to the quality and reliability of this work.

REFERENCES

[1] V. N. Batchvarov, "The Brugada Syndrome - Diagnosis, Clinical Implications and Risk Stratification," *Eur. Cardiol.*, vol. 9, no. 2, pp. 82–87, Dec. 2014.

[2] J. E. Romero, D. L. Li, R. Avendano, J. C. Diaz, R. Tung, and L. Di Biase, "Brugada Syndrome: Progress in Genetics, Risk Stratification and Management," *Arrhythmia Electrophysiol. Rev.*, vol. 8, no. 1, pp. 19–27, 2019.

[3] I. P. Popa, D. N. Șerban, M. A. Mărănducă, I. L. Șerban, B. I. Tamba, and I. Tudorancea, "Brugada syndrome: from molecular mechanisms and genetics to risk stratification," *Int. J. Mol. Sci.*, vol. 24, no. 4, p. 3328, 2023.

[4] R. Lahti, J. Rankinen, M. Eskola, K. Nikus, and J. Hernesniemi, "Intraventricular conduction delays as a predictor of mortality in acute coronary syndromes," *Eur. Heart J. Acute Cardiovasc. Care*, vol. 12, no. 7, pp. 430–436, 2023.

[5] L. Melo *et al.*, "Deep learning unmasks the ECG signature of Brugada syndrome," *PNAS Nexus*, vol. 2, no. 11, p. pgad327, 2023.

[6] P. Brugada and J. Brugada, "Right bundle branch block, persistent ST segment elevation and sudden cardiac death: a distinct clinical and electrocardiographic syndrome," *J. Am. Coll. Cardiol.*, vol. 20, no. 6, pp. 1391–1396, 1992.

[7] H. Watanabe and T. Minamino, "Genetics of Brugada syndrome," *J. Hum. Genet.*, vol. 61, no. 1, pp. 57–60, 2016.

[8] A. D. Krahn *et al.*, "Brugada syndrome," *Clin. Electrophysiol.*, vol. 8, no. 3, pp. 386–405, 2022.

[9] A. A. Wilde *et al.*, "Proposed diagnostic criteria for the Brugada syndrome: consensus report," *Circulation*, vol. 106, no. 19, pp. 2514–2519, 2002.

[10] J. Sieira, G. Dendramis, and P. Brugada, "Pathogenesis and management of Brugada syndrome," *Nat. Rev. Cardiol.*, vol. 13, no. 12, pp. 744–756, 2016.

[11] S. G. Priori *et al.*, "2015 ESC Guidelines for the management of patients with ventricular arrhythmias and the prevention of sudden cardiac death," *Europace*, vol. 17, no. 11, pp. 1601–1687, 2015.

[12] M. C. Gonzalez Corcia, C. de Asmundis, G. B. Chierchia, and P. Brugada, "Brugada syndrome in the paediatric population: a comprehensive approach to clinical manifestations, diagnosis, and management," *Cardiol. Young*, vol. 26, no. 6, pp. 1044–1055, 2016.

[13] C. M. Liu *et al.*, "A deep learning–enabled electrocardiogram model for the identification of a rare inherited arrhythmia: Brugada syndrome," *Can. J. Cardiol.*, vol. 38, no. 2, pp. 152–159, 2022.

[14] V. Randazzo *et al.*, "A vision transformer model for the prediction of fatal arrhythmic events in patients with Brugada syndrome," *Sensors*, vol. 25, no. 3, p. 824, 2025.

[15] S. Liao *et al.*, "Use of wearable technology and deep learning to improve the diagnosis of Brugada syndrome," *Clin. Electrophysiol.*, vol. 8, no. 8, pp. 1010–1020, 2022.

[16] I. Doundoulakis *et al.*, "Catheter ablation as an adjunctive therapy to ICD implantation in Brugada Syndrome," *Eur. Heart J. Qual. Care Clin. Outcomes*, vol. 10, no. 7, pp. 590–601, 2024.

[17] GE Healthcare Italia. [Online]. Available: https://www.gehealthcare.it

[18] S. Caligari, V. Randazzo, C. Giustetto, F. Gaita, and E. Pasero, "Predictive recognition of Brugada syndrome patterns in digital signal data using neural networks," in *Neural Networks: Overview of Current Theories and Applications*, in press.

[19] D. Bahdanau, K. Cho, and Y. Bengio, "Neural machine translation by jointly learning to align and translate," arXiv preprint arXiv:1409.0473, 2014.